Proceedings of the ASME/JSME 2011 8th Thermal Engineering Joint Conference
AJTEC2011
March 13-17, 2011, Honolulu, Hawaii, USA

AJTEC2011- 44570

THERMAL CONTACT RESISTANCE AT A METAL FOAM-SOLID SURFACE INTERFACE

Ehsan Sadeghi
University of Victoria
Victoria, BC, Canada

Scott Hsieh
Simon Fraser University
Burnaby, BC, Canada

Majid Bahrami
Simon Fraser University
Surrey, BC, Canada

ABSTRACT

Accurate information on heat transfer and temperature distribution in metal foams is necessary for design and modeling of thermal-hydraulic systems incorporating metal foams. The analysis of this process requires determination of the effective thermal conductivity as well as the thermal contact resistance (TCR) associated with the interface between the metal foams and adjacent surfaces/layers.

In the present study, a test bed that allows the separation of effective thermal conductivity and thermal contact resistance in metal foams is described. Measurements are performed in a vacuum under varying compressive loads using ERG Duocel aluminum foam samples with different porosities and pore densities. Also, a graphical method associated with a computer code is developed to demonstrate the distribution of contact spots and estimate the real contact area at the interface. Our results show that the porosity and the effective thermal conductivity remain unchanged with the variation of compression in the range of 0 to 2 MPa; but TCR decreases significantly with pressure due to an increase in the real contact area at the interface. Moreover, the ratio of real to nominal contact area varies between 0 to 0.013, depending upon the compressive force, porosity, and surface characteristics.

INTRODUCTION

Transport phenomena in porous media have been the focus of many industrial and academic investigations [1-4]. The majority of the studies reported in the literature deal with low porosity media such as granular materials and packed beds [1, 2]. Over the last decade, high porosity micro-structures such as open-cell metal foams have received more attention. Interest in these media stems from their relatively low cost, ultra-low density, high surface area to volume ratio, and their ability to mix the passing fluid. These features are highly desirable for a wide variety of applications including microelectronics cooling, aerospace technology, filtration, heating, and compact heat exchangers [3-7]. In majority of these applications, there is an interface between the foam and a solid surface which gives rise to an important phenomenon called thermal contact resistance (TCR) acting against heat transfer in metal foams. Due to high porosity and roughness of the free surface of metal foams, the actual contact area at the interface with a solid surface is very small; this emphasizes the significance of TCR in metal foam-solid surface interface. In some applications, metal foams are brazed to a metallic sheet which may create a perfect contact, but because of high porosity of the medium, TCR still exists due to constriction and spreading of the heat flow passing through the metal plate-foam interface.

A review of the literature indicates that in all previous studies related to heat transfer in metal foams, e.g. [8-15], the TCR was neglected due to attachment to a metallic sheet or 'bundled up' with the effective thermal conductivity and only effective thermal conductivity values were reported. One fundamental issue with combining the two is that TCR is an *interfacial phenomenon* that is a function of mechanical load and surface characteristics and thermal conductivity of both interfacing surfaces, whereas thermal conductivity is a transport coefficient characterizing the *bulk* medium. Thermal conductivity and TCR should therefore be distinguished. Furthermore, the effect of compression on thermal conductivity and TCR has not been thoroughly investigated.

The objective of this study is to measure the thermal conductivity and contact resistance of metal foams and estimate the size and distributions of contact spots (real contact area) at the interface. The experimental technique developed in this

study allows the deconvolution of TCR and thermal conductivity and was used to perform a comprehensive experimental study to determine the effective thermal conductivity and TCR at different compressive loads.

A custom-made test bed was designed and built that enables the measurements of thermal conductivity and TCR of porous media at different air pressures. The test bed was equipped with a loading mechanism that allows the application of various compressive loads on the samples. ERG Duocel aluminum foams with various porosities and pore densities are used in the experiments. The tests are performed under a vacuum and the test column is surrounded by an aluminum radiation shield to limit the radiation heat losses. Thus, neglecting the radiation losses, the only heat transfer mechanism is conduction through the solid ligaments of metal foams. The effective thermal conductivity and TCR are deduced from the total thermal resistance measurements by performing a series of experiments with aluminum foam samples of various thickness and similar micro-structure, i.e. porosity and pore density. Effects of compression, porosity, and pore density are studied on the effective thermal conductivity and TCR.

To estimate the actual contact area at the metal foam-solid interface, a pressure sensitive carbon paper is placed between the foam and the solid surface to print the contact spots at different compressive loads. A computer code is then developed using MATLAB to analyze the produced images and calculate the size and distribution of contact spots.

THERMAL CONDUCTIVITY AND TCR MEASUREMENT

The schematic of the test bed for thermal measurements is shown in Fig. 1. The test chamber consists of a stainless steel base plate and a bell jar enclosing the test column. The test column consists of, from top to bottom: the loading mechanism, the steel ball, the heater block, the upper heat fluxmeter, the sample, the lower fluxmeter, the heat sink (cold plate), the load cell, and the poly methyl methacrylate (PMMA) layer. The heater block consists of circular flat copper in which cylindrical pencil-type electrical heaters are installed. The designed cold plate consists of a hollow copper cylinder, *1.9 cm* high and *15 cm* diameter. Cooling is accomplished using a closed loop water-glycol bath in which the coolant temperature can be set. The cold plate is connected to the chiller unit which adjusts the cold water temperature. A *1000 lbs* load cell is used to measure the applied load to the sample. The fluxmeters were made of a standard electrolyte iron material. In this study, the cold plate temperature and the power of the electrical heater were set on *0°C* and *12 W*, respectively.

To measure temperatures six T-type thermocouples were attached to each fluxmeter at specific locations shown in Fig. 1. The thermocouples were located *5 mm* apart with the first one *10 mm* from the contact surface. The thermal conductivity of the iron fluxmeter was known and used to measure the heat flow rate transferred through the contact interface. The samples used in this study were open-cell aluminum foams. These Duocel foams were produced through a proprietary process developed by ERG in which the resulting foam has the identical chemical composition of the base alloy used. The foam was made from aluminum alloys of *6101* and cut in cylindrical shapes with the diameter of *25 mm* and then polished. Aluminum foams with the porosity range of *90* to *96%* and pore density of *10* and *20 PPI* were used in this study.

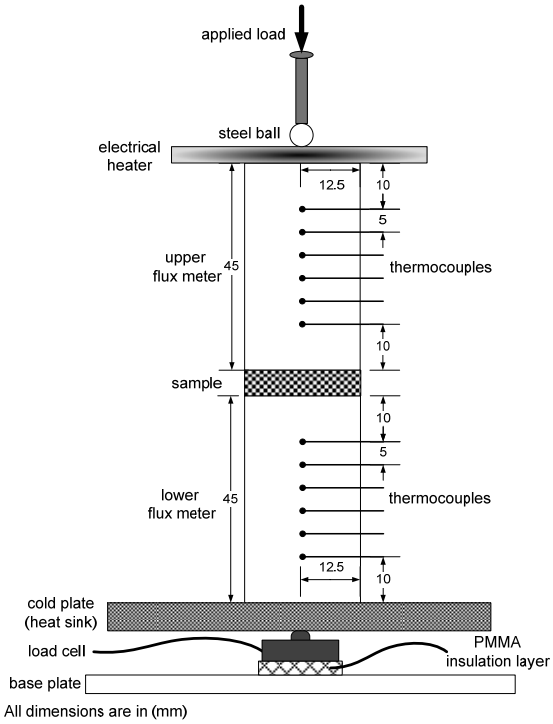

FIGURE 1. SCHEMATIC VIEW OF THE TEST BED FOR THERMAL MEASUREMENT

Test Procedure

To study heat conduction only through the solid ligaments and contact surfaces, experiments were conducted under a vacuum. A vacuum level of 10^{-5} *mbar* was achieved under the test chamber using a vacuum machine. Temperatures and pressure were recorded at various compressive loads when steady-state conditions were achieved; to reach thermal equilibrium all the experiment's parameters were kept constant and carefully monitored for approximately *4-5* hours for each data point. The effects of compression were investigated over the range of *0.3 to 2 MPa*.

The temperature gradient between the hot and cold plates results in essentially one-dimensional heat conduction from the top to the bottom of the test column. Radiation heat transfer between the sample and the fluxmeters is also negligible since the absolute temperature levels in the samples during the tests remain relatively low, i.e. less than *100°C* (*373 K*). Thus, the

heat transferred through the fluxmeters is only due to conduction and can be determined using Fourier's equation.

$$Q = -kA\frac{dT}{dz} \quad (1)$$

where, dT/dz is the temperature gradient along the test column, k is the thermal conductivity of the fluxmeters, and A is the cross-sectional area of samples/fluxmeters. The temperatures at the top and bottom contact surfaces can be extrapolated through the measured heat flux. The measured total thermal resistance at each pressure, R_{tot}, includes the sample (bulk) thermal resistance and the thermal contact resistance (at the top and bottom interfaces) and can be expressed as:

$$R_{tot} = R_{MF} + TCR = \frac{\Delta T_{ul}}{Q} \quad (2)$$

where, ΔT_{ul} is the temperature difference between the upper and the lower contact surfaces. R_{MF} and TCR are the metal foam resistance and the total contact resistance (summation of contact resistance at the top and the bottom surfaces), respectively.

To deconvolute thermal conductivity and TCR, two experiments were performed with samples of different thicknesses; but with identical micro-structural parameters. Due to identical micro-structure and solid surface characteristics at the top and the bottom interfaces, contact resistances for both samples can be considered equal at the same pressure. Applying Eqn. (2) to both measurements and subtracting them yields the effective thermal conductivity:

$$k_{eff} = \frac{t_1}{R_{MF1}A} = \frac{t_2}{R_{MF2}A} \quad (3)$$

$$k_{eff} = \frac{t_1 - t_2}{(R_{tot1} - R_{tot2})A} \quad (4)$$

where, $t_1$and t_2 are the thicknesses of sample 1 and 2 respectively at the specific applied pressure, and A is the cross-section of the samples. The two thickness values for the experiments are *13.92± 0.03 mm* and *17.93± 0.03 mm*. To investigate the effect of compression on the sample thickness, different Al foam samples with different porosities and pore densities were compressed step by step using a standard tensile-compression machine. Thickness variation was measured for all of the samples at different pressures from *0* to *2 MPa* using a Mitutoyo digital micrometer with the accuracy of *1 μm*. The results show that the maximum thickness variation is less than *1.5%* that can be neglected. Equation (4) can be used to find the effective thermal conductivity; the TCR can then be calculated by Eqn. (2).

Uncertainty Analysis

Considering the relationships for evaluating the effective thermal conductivity and the thermal contact resistance, i.e. Eqn.(4) and Eqn.(2), the relevant parameters in the analysis can be expressed as:

$$R_{tot} = f(Q, \Delta T, t, A, P_c, \phi_s) \quad (5)$$

The main uncertainty in these experiments is due to errors in determining the heat flux through the sample which leads to a maximum error of *3.2%*. The maximum uncertainties for the thermocouples and the data acquisition readings are *±1°C* which introduces a maximum error of *1.7%* between the interfaces of the sample and fluxmeters. To include the uncertainty in micro-structure similarity of the samples used in two sets of experiments, the relative density of the samples with different thicknesses was measured and the difference was used as a representative of the morphology uncertainty. This uncertainty as well as those associated with the load cell, thickness, and cross-sectional area measurements and are listed in Tab. 1. The maximum uncertainty for the thermal resistance measurements can be calculated from [16]:

$$\frac{\delta R_{tot}}{R_{tot}} = \sqrt{\left(\frac{\delta Q}{Q}\right)^2 + \left(\frac{\delta \Delta T}{\Delta T}\right)^2 + \left(\frac{\delta t}{t}\right)^2 + \left(\frac{\delta A}{A}\right)^2 + \left(\frac{\delta P_c}{P_c}\right)^2 + \left(\frac{\delta \phi_s}{\phi_s}\right)^2} \quad (6)$$

For the present study, the maximum uncertainty is estimated to be ± *5%*.

TABLE 1. UNCERTAINITY OF PARAMETERES INVOLVED IN THE ANALYSIS

$\delta Q/Q$	$\delta \Delta T/\Delta T$	$\delta t/t$	$\delta A/A$	$\delta P_c/P_c$	$\delta \phi_s/\phi_s$
3.2%	1.7%	0.5%	0.8%	2.5%	2.2%

MORPHOLOGY OF CONTACT SPOTS

To find the size and distribution of contact spots, a sheet of carbon copy paper along with a white paper was placed on top and bottom of the samples. The assembly was compressed in a standard tensile-compression machine and the contact spots were printed on the white paper. The printed images were captured with a high resolution camera. An image processing technique implemented in MATLAB enabled accurate evaluation of the contact area at the metal foam-solid interface. The image was first masked with green color that highlighted the area of interest in a given RGB image shown in Fig. 2.

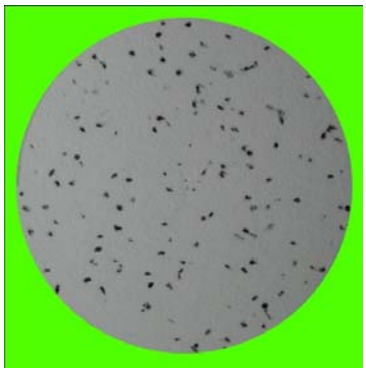

FIGURE 2. MASKED IMAGE, AL FOAM WITH 95.3% POROSITY AND 20 PPI PORE DENSITY AT P_c=1.53MPa

By analyzing the green channel of the RGB image, the total pixel count/area of the sample material can be found. Once the circular area of interest was found, the RGB image was converted into an 8-bit greyscale image where contact point can be extracted through image filtering by contrast. The contact points were seen as dark spots in the image, where lighter shades of grey were shadows or blur caused by the camera. To differentiate contact spots and shadows, each pixel in the image was compared to their neighbouring pixels as seen in Fig. 3. Each pixel was individually scanned in a cross pattern as seen in Fig. 3 (a), the pixel in the center of the cross was compared with the pixel directly above, below, left and right. The dark/lightness of the gradient was being monitored while contrast was being analyzed simultaneously. The centering pixel in Fig. 3 (a) appeared to be dark grey, and there is a change in its contrast with the surrounding pixels, hence, it is almost definite that this particular spot is a shadow and not a contact point. However, in Fig. 3 (b), the center pixel met both requirements of being dark enough and having a negligible change in contrast with the neighbouring pixels; therefore, this location can be said to be a contact point. Each contact point was then highlighted with a different color which is shown in Fig. 4.

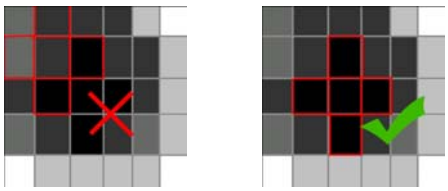

(a) (b)

FIGURE 3. CONTRAST FILTERING

After scanning through the entire image, the pixel count of the contact spot is compared with the total area of the boundary circle, and then contact area ratio is calculated.

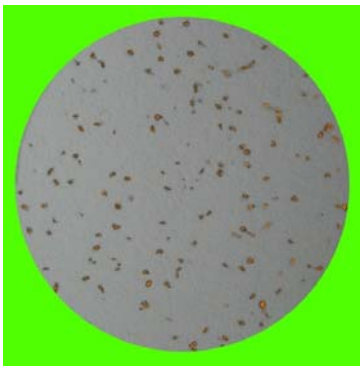

FIGURE 4. HIGHLIGHTED CONTACT POINTS, AL FOAM WITH 95.3% POROSITY AND 20 PPI PORE DENSITY AT P_c=1.53MPa

RESULTS AND DISCUSSION

The measurements were taken at different compressive loads in a vacuum to study the effects of compressive load on TCR and effective thermal conductivity. Also, to find the actual contact area at the metal foam-solid surface interface, separate compression tests were performed and the produced images were analyzed using the developed image processing technique.

Figure 5 shows the variation of the effective thermal conductivity with compression at different porosities and pore densities. The effective conductivity decreases with an increase in the porosity; however, the effect of pore density seems to be insignificant. Lower porosity values are associated with a higher volume of conductive materials which provides high conductive paths for the heat flow. Also, the effect of compressive load on the thermal conductivity is insignificant over the studies pressure range. Our measurements show that the highest deformation occurred under the compression is *1.4%* which does not have a significant impact on the micro-structure; however, higher compressive loads, which produce larger deformations, may reduce the thermal conductivity in the direction of compression as reported in [4].

Present experimental data are compared with existing experimental data in Fig. 6. Majority of existing data [9-11, 14] were reported for Al foam-air; but since the thermal conductivity of air very low, its contribution in the effective thermal conductivity is negligible. The compressive load for the existing experimental data was not reported; therefore, the mean value of the present data at different compressive loads is used for a comparison. As shown, the present experimental data agree with the majority of existing data at different porosities; Paek et al. [9] data underestimates the effective thermal conductivity. It should be noted that the data used for the comparison belong to the samples, which were brazed to Al sheets and the temperatures of Al sheets near the contact points were used for evaluating the thermal conductivity, i.e. TCR for these data was negligible.

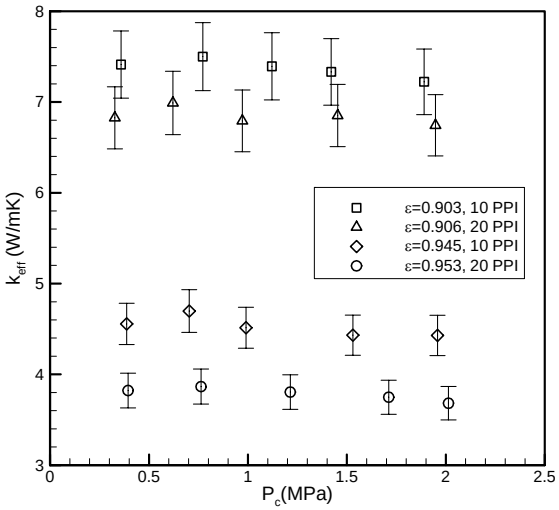

FIGURE 5. EFFECTIVE THERMAL CONDUCTIVITY OF DIFFERENT AL FOAM SAMPLES OVER A WIDE RANGE OF COMPRESSION

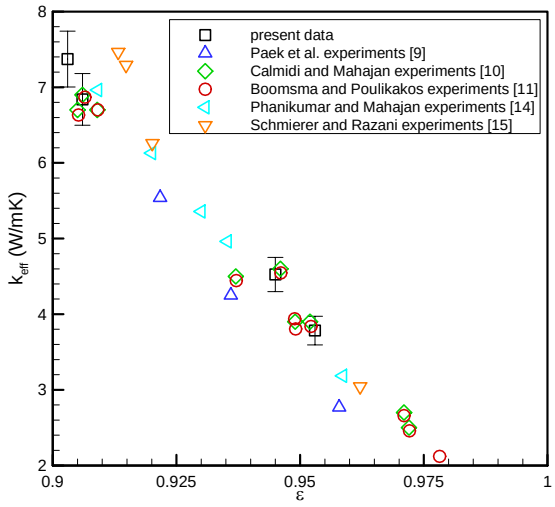

FIGURE 6. PRESENT EXPERIMENTAL DATA FOR AL FOAM-VACUUM IN COMPARISON WITH EXISTING EXPERIMENTAL DATA FOR AL FOAM-AIR (DATA OF REF. [15] IS FOR AL FOAM-VACUUM)

Figure 7 shows the thermal contact resistance of the examined Al foam samples at different compressive loads. It can be seen that TCR is more sensitive to the compressive load rather than the porosity and pore density. The contact area increases with an increase in the compressive load which results in a significant reduction of TCR. Also, samples with higher porosities have lower solid material in contact region which results in a higher TCR. Furthermore, the number of contact spots increases with an increase in the pore density; however, these contact spots have a smaller size and different surface profile. As a result of these competing effects, the effect of pore density on contact resistance is not significant.

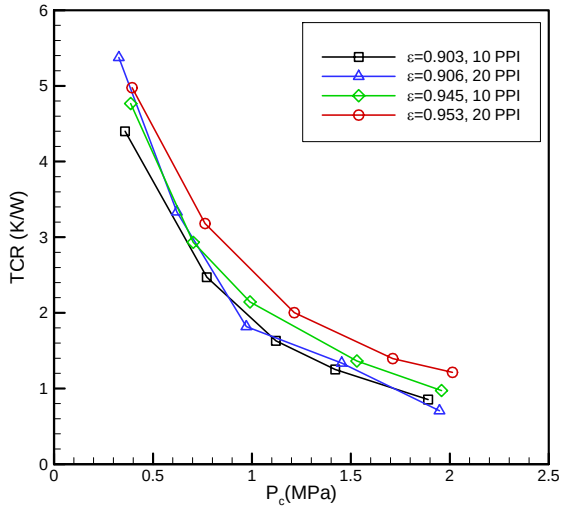

FIGURE 7. TCR OF DIFFERENT AL FOAM SAMPLES OVER A WIDE RANGE OF COMPRESSION

Distribution of contact spots for different Al foam samples is shown in Fig. 8 for moderate and high pressures. As shown, the total contact area increases with an increase in the foam density. Also, higher pore densities provide a larger number of contact points which can reduce the TCR as shown in Fig. 7. The ratio of real to nominal contact area η, which is found from the analysis of the printed images, is shown in Fig. 9; the nominal contact area was considered equal as the cross-sectional area. There is a small difference between the contact area ratio of the bottom and top surfaces due to different distribution of ligaments on these surfaces, therefore, in our analysis the average contact area ratio is considered.

Reviewing Figs. 7-9 shows that for a relatively high pressure, the number and total area of contact spots increase with an increase in the pore density and foam density which results in a reduction of the TCR; however, in low contact pressure, $P_c < 0.5\ MPa$, the contact surface morphology, e.g. roughness, becomes more important and dominates the effects of pore density and porosity. Therefore, the smaller contact area (higher TCR) of denser foams such as the foam with $\varepsilon=0.906$ can be due to a higher surface roughness.

Figure 10 shows the TCR to total thermal resistance ratio of examined Al foam samples with the average thickness of *13.92 mm* at different compressive loads. TCR is the dominant resistance at low compressive loads, $P_c < 0.3\ MP$, contributing more than *50%* of the total resistance. This contribution decreases for all the samples with an increase in the compressive load. Both foam bulk resistance and TCR increase with an increase in porosity, but this variation is higher for the foam bulk resistance. Therefore, the TCR to total thermal resistance ratio decreases at higher porosities.

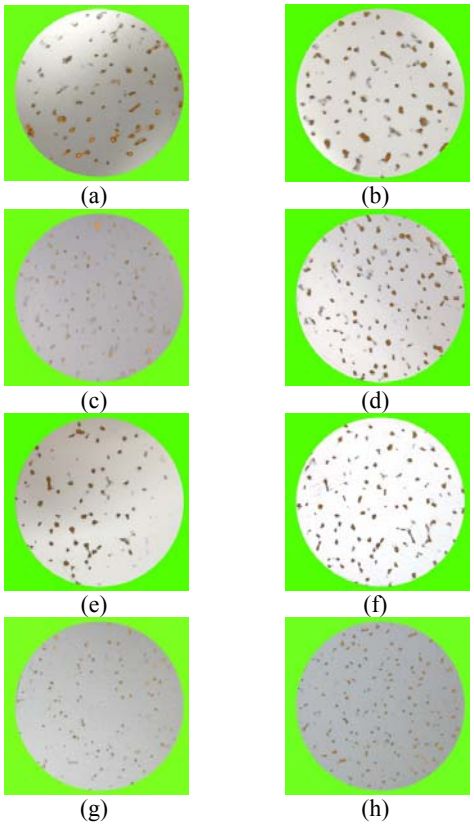

FIGURE 8. HIGHLIGHTED CONTACT POINTS FOR VARIOUS AL FOAM SAMPLES: (a) ε =90.3%, 10 PPI AT P_c=1.43 MPa; (b) ε =90.3%, 10 PPI AT P_c=2.85 MPa; (c) ε =90.6%, 20 PPI AT P_c=1.02 MPa; (d) ε =90.6%, 20 PPI AT P_c=2.44 MPa; (e) ε =94.5%, 10 PPI AT P_c=1.32 MPa; (f) ε =94.5%, 10 PPI AT P_c=3.06 MPa; (g) ε =95.3%, 20 PPI AT P_c=1.02 MPa; (h) ε =95.3%, 20 PPI AT P_c=3.06 MPa

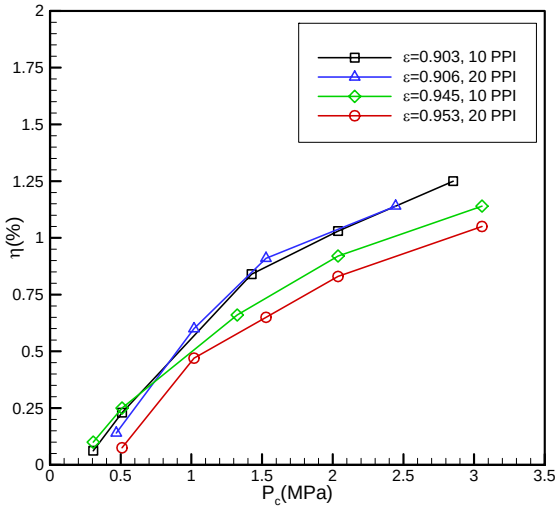

FIGURE 9. TOTAL CONTACT AREA TO CROSS-SECTIONAL AREA RATIO FOR VARIOUS AL FOAM SAMPLES UNDER COMPRESSION

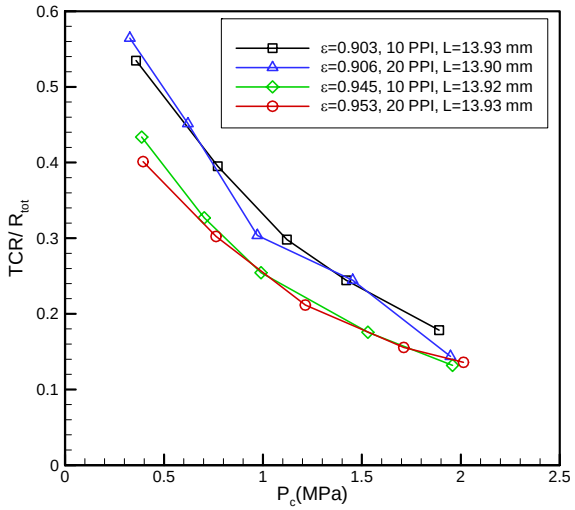

FIGURE 10. TCR TO TOTAL THERMAL RESISTANCE RATIO FOR VARIOUS AL FOAM SAMPLES UNDER COMPRESSION

SUMMARY AND CONCLUSIONS

A test bed was designed and built to measure the thermal conductivity and thermal contact resistance of metal foams under various compressive loads. Also, a computer program associated with an experimental set-up was developed to find the distribution and total size of actual contact area at the metal foam-solid surface interface. The analytical modeling of thermal conductivity and thermal contact resistance will be provided a companion paper. The present experimental data for the effective thermal conductivity are in good agreement with existing data over a range of porosities. Our results show that the effective thermal conductivity increases with an increase in the foam density, but it is relatively insensitive to compressive load in the range of *0-2 MPa*.

An important finding is the large contribution of thermal contact resistance to the total thermal resistance, more than *50%*, for relatively low compressive loads. The high values of TCR are related to very small ratio of contact area to the cross-sectional area; the maximum ratio is *1.25%* at the contact pressure of *3 MPa*. TCR is more sensitive to the compressive load rather than the porosity and pore density; however, it slightly decreases with an increase in the foam density.

This work provided new insights on the importance of thermal contact resistance and has helped clarify the impact of this key interfacial phenomenon on the thermal analysis of metal foams.

ACKNOWLEDGMENTS

The authors are grateful for the financial support of the Natural Sciences and Engineering Research Council (NSERC) of Canada, and the Canada Research Chairs Program. The

authors would like to thank Dr. Ned Djilali for his financial support and useful suggestions during the work.

REFERENCES

[1] Kaviany, M., 1995. *Principles of Heat Transfer in Porous Media*. 2nd ed., Springer, New York, US.

[2] Bahrami, M., Yovanovich, M. M., and Culham, J. R., 2006. "Effective Thermal Conductivity of Rough Spherical Packed Beds". *Int. J. Heat Mass Transfer*, **49**, pp. 3691-3701.

[3] Dukhan, N., Picon-Feliciano, R., and Alvarez-Hernandez, A. R., 2006. "Heat Transfer Analysis in Metal Foams with Low Conductivity Fluids". *J. Heat Transfer*, **128**(8), pp. 784-792.

[4] Ozmat, B., Leyda, B., and Benson, B., 2004. "Thermal Applications of Open-Cell Metal Foams". *Materials and Manufacturing Processes*, **19**(5), pp. 839-862.

[5] Bhattacharya, A., Calmidi, V. V., and Mahajan, R. L., 2002. "Thermophysical Properties of High Porosity Metal Foams", *Int. J. Heat Mass Transfer*, **45**, pp. 1017-103.

[6] Hunt, M. L., and Tien, C. L., 1988. "Effects of Thermal Dispersion on Forced Convection in Fibrous Media", Int. J. Heat Mass Transfer, **31**, pp. 301-309.

[7] Mahjoob, S., Vafai, K., 2008. "A Synthesis of Fluid and Thermal Transport Models for Metal Foam Heat Exchangers". *Int. J. Heat Mass Transfer*. **51**, pp. 3701-3711.

[8] Calmidi, V. V., 1998. "Transport Phenomena in High Porosity Metal Foams". Ph.D. Thesis, University of Colorado, Boulder, CO.

[9] Kim, S. Y., Paek, J. W., and Kang, B. H., 2000. "Flow and Heat Transfer Correlations for Porous Fin in a Plate-Fin Heat Exchanger". *ASME J. Heat Transfer*, **122**, pp. 572-578.

[10] Calmidi, V. V., and Mahajan, R. L., 1999. "The Effective Thermal Conductivity of High Porosity Fibrous Metal Foams", *J. Heat Transfer*, **121**(2), pp. 466-471.

[11] Boomsma, K., and Poulikakos, D., 2001. "On The Effective Thermal Conductivity of a Three-Dimensionally Structured Fluid-Saturated Metal Foam". *Int. J. Heat Mass Transfer*. **44**, pp. 827-836.

[12] Krishnan, S., Garimella, S., and Murthy, J.Y., 2008. "Simulation of Thermal Transport in Open-Cell Metal Foams: Effects of Periodic Unit-Cell Structure". *J. Heat Transfer*, **130**(2), pp. 024503-024507.

[13] Babcsan, N., Meszaros, I., and Heman, N., 2003. "Thermal and Electrical Conductivity Measurements on Aluminum Foams". *Materialwiss. Werkstofftech*, **34**, pp.391-394.

[14] Phanikumar, M.S., and Mahajan, M.L., 2002. "Non-Darcy Natural Convection in High Porosity Metal Foams". *Int. J. Heat Mass Transfer*. **45**, pp. 3781-3793.

[15] Schmierer, E.N., and Razani, A., 2006. "Self-Consistent Open-Celled Metal Foam Model for Thermal Applications". *J. Heat Transfer*, **128**, pp. 1194-1203.

[16] Taylor, J.R., 1997. *An Introduction to Error Analysis: The Study of Uncertainties in Physical Measurements*. 2nd ed., Chap. 3, University Science Books, Sausalito, US.